REPORT DOCUMENTATION PAGE

Form Approved OMB No. 0704-0188

1. AGENCY USE ONLY *(Leave blank)*	2. REPORT DATE	3. REPORT TYPE AND DATES COVERED
	19.Jun.06	MAJOR REPORT

4. TITLE AND SUBTITLE
THE RELATIONSHIP BETWEEN CLOUD-TO-GROUND LIGHTNING AND PRECIPITATION ICE MASS: A RADAR STUDY OVER HOUSTON.

5. FUNDING NUMBERS

6. AUTHOR(S)
MAJ GAUTHIER MICHAEL L

7. PERFORMING ORGANIZATION NAME(S) AND ADDRESS(ES)
UNIVERSITY OF ALABAMA HUNTSVILLE

8. PERFORMING ORGANIZATION REPORT NUMBER
CI04-1788

9. SPONSORING/MONITORING AGENCY NAME(S) AND ADDRESS(ES)
THE DEPARTMENT OF THE AIR FORCE
AFIT/CIA, BLDG 125
2950 P STREET
WPAFB OH 45433

10. SPONSORING/MONITORING AGENCY REPORT NUMBER

11. SUPPLEMENTARY NOTES

12a. DISTRIBUTION AVAILABILITY STATEMENT
Unlimited distribution
In Accordance With AFI 35-205/AFIT Sup 1

DISTRIBUTION STATEMENT A
Approved for Public Release
Distribution Unlimited

12b. DISTRIBUTION CODE

13. ABSTRACT *(Maximum 200 words)*

14. SUBJECT TERMS	15. NUMBER OF PAGES
	19
	16. PRICE CODE

17. SECURITY CLASSIFICATION OF REPORT	18. SECURITY CLASSIFICATION OF THIS PAGE	19. SECURITY CLASSIFICATION OF ABSTRACT	20. LIMITATION OF ABSTRACT

The Relationship Between Cloud-to-Ground Lightning and Precipitation Ice Mass: A Radar Study over Houston

Michael L. Gauthier*

Department of Atmospheric Science, Global Hydrology and Climate Center, The University of Alabama in Huntsville, Huntsville, Alabama, 35899 USA

Walter A. Petersen

ESSC/NSSTC University of Alabama Huntsville
Huntsville, Alabama 35899

Lawrence D. Carey
Department of Atmospheric Sciences, Texas A&M University
College Station, Texas 77843

Hugh J. Christian Jr.

ESSC/NSSTC University of Alabama Huntsville
Huntsville, Alabama 35899

---

* - The views expressed in this paper are those of the author and do not reflect the official policy or position of the U.S. Air Force, Department of Defense or the U.S. Government.

ABSTRACT.

Using seven summer-seasons (1997-2003, over 46,000 volumes) of NEXRAD data, coincident climatologies of summer-season ground flash densities and radar derived, column integrated, precipitation ice mass (IM) were developed, extending global studies of IM and lightning to more regional and cell scales around Houston, TX. Results indicate that local maximums in cloud-to-ground (CG) lightning were indeed accompanied by peaks in IM. Extending previous global findings to cell-scales, we establish a link between a storms ability to generate enhanced concentrations of mixed-phase IM, and its ability to generate lightning. Relative to the documented CG lightning "anomaly" over Houston, these results imply that unique aspects of the Houston urban area must first generate an anomaly in convective intensity and precipitation ice, thereby generating an anomaly in lightning; causal hypotheses must be capable of explaining either increased frequency and/or intensity of convection, and then relating these to the enhancement of IM and lightning production.

INDEX TERMS

3304 Atmospheric electricity
3324 Lightning
3309 Climatology
3329 Mesoscale meteorology
3360 Remote sensing
6952 Radar atmospheric physics

1. Introduction

Through numerous laboratory, in-situ, remote sensing, and modeling studies [cf. MacGorman and Rust, 1998], it is generally accepted that clouds become significantly electrified and produce lightning when sufficient numbers of ice crystals collide with graupel particles in the presence of super-cooled water via the non-inductive charging (NIC) mechanism [e.g., Takahashi, 1978; Saunders et al., 1991]. The particle-cloud scale physics associated with NIC assert *three key requirements for thunderstorm electrification and subsequent lightning production*: (1) the existence of convective updrafts, capable of (2) driving robust mixed-phase precipitation ice processes (i.e., production of graupel/hail and smaller ice crystals/splinters); and the occurrence of resultant (3) rebounding graupel-ice crystal collisions in the presence of super-cooled cloud water. Although these three ingredients are critical to the thunderstorm electrification process, it is clear that (2) and (3) can not proceed without the presence of a significant convective updraft. Indeed from an energetics standpoint, stronger updrafts should be capable of producing more lightning.

Further, there appear to be localized enhancements of ground flash densities in and around various urban areas, specifically the Houston metropolitan area [e.g., Orville et al., 2001; Steiger et al., 2002; Gauthier et al., 2005]. Therefore, we postulate that the unique aspects of the Houston urban area must first generate an anomaly in precipitation ice mass (similar to those observed globally; [Petersen et al., 2005]), via localized enhancements in cloud forcing, which then generates the observed anomaly in cloud-to-ground (CG) lightning. Utilizing Weather Surveillance Radar-1988 Doppler (WSR-88D) data collected at the League City, TX (KHGX) radar site, we establish a physical link between the occurrence of CG lightning and the presence of enhanced precipitation ice mass in the mixed phase region of the atmosphere (-10° C to -40°

C, hereafter referred to as the "charging zone" – the area enclosing the region about which active NIC likely occurs; [Takahashi, 1978; Saunders et al., 1991]) over and around the Houston area.

2. Data and Method

Seven years (1997-2003) of archived (Level II) KHGX radar data obtained from the National Climatic Data Center (NCDC) were analyzed for the warm season (June – August; JJA) daylight hours (0900 – 1859 CDT). These archived data consist of volumetric measurements of radar reflectivity (Z), radial velocity and spectrum width. To adequately sample the atmosphere, the WSR-88D employs several scanning strategies or Volume Coverage Patterns (VCPs), each having its own utility based on a given weather scenario (i.e., non-precipitating "Clear Air", "Precipitation", "Severe Weather", etc.).

To investigate the relationship between precipitation-sized ice in the charging zone (approximately 7-11 km above ground level, based on NCEP reanalysis for this climatological period [Kalnay et al., 1996]) and the location (intensity) of NLDN detected lightning ground strikes (flash densities) we desire radar coverage that adequately samples those levels of the atmosphere. The proximity of the Houston area to the radar (approximately 40 km from city center to KHGX) coupled with the climatological altitude of the charging zone dictate the use of radar volumes collected while the radar was scanning to higher elevation angles, thereby sampling the upper portions of the atmosphere at ranges closer to the radar. Of the available VCPs, the scanning strategy employed in VCP-11 ("Severe Weather") mode provides the best vertical sampling, relative to the geometry of the problem at hand, sweeping out a total of 14 elevation scans in 5 minutes. Of the 55,571 available volumes (all VCPs), over 83% were

collected in VCP-11 mode, providing a dataset of 46,479 volumes from which our analyses were conducted.

Each of the VCP-11 volumes were converted from their native (Level II) format to UF (Universal Format; [Barnes, 1980]), and then interpolated onto a 150 x 150 x 20 (x, y, z) Cartesian grid (centered on KHGX) using the National Center for Atmospheric Research (NCAR) REORDER software package [Mohr et al., 1986] with horizontal (x,y) and vertical (z) grid resolutions being 2 km and 1 km, respectively. In order to minimize erroneous data-pairs resulting from missing, and/or poorly sampled data, the radar analysis was only performed for pixels at a range in excess of 15 km from the KHGX radar (i.e., outside of the "cone of silence") and within 150 km of the radar.

Estimations of the precipitation ice mass (M) in each volume were then made by applying the following M-Z relationship to all valid 4 km^3 pixels located between z = 7 and 11 km:

$$M = 1000\pi\rho_i N_0^{3/7}\left(\frac{5.28\times10^{-18}}{720}Z\right)^{4/7} \text{ g m}^{-3}, \qquad (1)$$

where Z is in mm^6 m^{-3}, N_0 = 4 x 10^6 m^{-4}, and ρ_i = 917 kg m^{-3}. Note this particular M-Z relationship, first presented by Carey and Rutledge [2000], is for tropical convection, however it has since been applied to more regional [Petersen and Rutledge, 2001] and global [Petersen et al., 2005] lightning studies, with minor density alterations. Although many other Z-M relationships exist in the literature, reflecting variations in continentality, convective regime, and cloud system type [cf. Black, 1990] we feel justified in utilizing Equation 1 for the following reasons: (1) strong oceanic influences due to the proximity of the KHGX radar (and its domain) to the coast, coupled with prevailing onshore flow during the summer season, as dictated by the

climatological presence of the sub-tropical high pressure center, create an environment not overly dissimilar to that of a tropical island, distinctly different than mid-latitude continental conditions, and (2) the spatial and temporal trends in column integrated values of M (IM), as opposed to the computed values are what will be emphasized in this study. Furthermore, the use of Equation 1 will provide a consistent basis from which we can *extend the global results of Petersen et al. [2005] to regional and cell scales.*

Coincident with each radar volume, ground strike locations (i.e., flashes occurring from the beginning of one volume scan to the beginning of the subsequent volume scan) detected by the NLDN [Cummins et al., 1998] were gridded to match the horizontal dimensions of the Cartesian radar grid, with flash densities (FDs) calculated in flashes km^{-2} $hour^{-1}$. Note that we have chosen to disregard flashes with positive peak currents less than 10 kA following the recommendations of Cummins et al. [1998]. In this fashion we are able to correlate radar derived IM values with ground strike locations, and flash densities (FDs), observed by the NLDN.

Two separate *Eulerian* methods were used to compare warm-season statistics of IM and CG lightning, both of which mimic the approach taken by Petersen et al. [2005], who performed similar analyses on a global scale utilizing coincident data gathered by the precipitation radar (PR) and lightning imaging sensor (LIS) flown on the TRMM (Tropical Rainfall Mapping Mission) satellite. In the first method (the "ensemble" approach; EN) each individual radar volume was treated as a single data point with spatially integrated values of IM being correlated to observed FDs (each computed relative to the area of the entire domain). This approach yielded an ensemble sample size equal to the number of individual radar volumes processed, 46,479. The second approach compared time-integrated (TI) or cumulative means for each 2 km grid square within the domain by dividing the sum of the normalized IMs and flash counts (each normalized

by the pixel area, 4 km^2) by the number of summer seasons used in the analysis (seven). This method yielded a total of 17,560 data points for comparison (one for each valid 4 km^2 pixel within the horizontal analysis domain).

A third approach utilized an IDL (Interactive Data Language) variant of the Thunderstorm Identification, Tracking, Analysis and Nowcasting cell tracking algorithm (TITAN [Dixon and Wiener, 1993]) to perform a *Lagrangian* analysis, comparing storm total IMs with storm flash counts (FCs) on a cell-by-cell basis. Here, we set the minimum storm size area and tracking altitude for identifying radar reflectivity cells as 12 km^2 (3 pixels) at an altitude of 2 km, with a threshold reflectivity value of 30 dBZ. Since IMs and FCs had previously been computed for each pixel in the dataset, cell totals of each parameter were taken as the sum of IMs and FCs associated with each pixel comprising the cell. Note this approach effectively treated each cell as a vertical entity, accounting for neither vertical tilt, nor ground flashes coming to ground in regions of reflectivity less than 30 dBZ. Applied to each volume within our radar dataset, the algorithm yielded a total of *676,153 cells for comparison allowing us to test (extend) the global results of Petersen et al. on (to) much smaller scales.*

3. Results and Discussion

Figure 1 presents an anomaly map of TI mean FDs (shaded contours) for ground strikes occurring over all volumes included in this study; here the TI mean FD for each pixel was normalized by the TI mean FD of the entire domain with values >1 (<1) being associated with positive (negative) anomalies. Overall, this seven-year seasonal mean FD anomaly map is similar to that of Gauthier et al. [2005, Figure 2a], with FDs in the vicinity of the Houston area approaching 2 to 3 times that of the domain mean. Regarding our IM-FD hypothesis, the white

contours in Figure 1 represent corresponding anomalies in radar derived ice mass (i.e., TI mean IM anomalies). In qualitative agreement with the findings of Petersen et al. [2005], a clear correspondence between the two variables is observed with areas of enhanced mean FDs spatially collocated near enhancements in mean IM indicating that precipitation ice mass in the charging zone and CG lightning are well correlated. To quantify this statement, we present scatter plots relating IM with lightning activity (not anomalies) for each analysis method: EN, TI and CT (Figures 2a – 2c, respectively). Consistent with the qualitative relationship identified in Figure 1, regardless of analysis technique, Figures 2a – 2c indicate strong positive correlations between IM and CG lightning, with linear correlation coefficients (R) of 0.72, 0.91 and 0.80 for the EN, TI and CT methods, respectively. As pointed out by Petersen et al. [2005], the unexplained variances (i.e., discrete bands of noise and scatter) found in these types of analyses are likely the result of sampling issues (both spatial resolution and instrumentation), coupled with the discrete nature of CG discharges. Relative to our analyses, primary deviations from a best fit line most likely arise: (1) when ground flashes initiated in the vicinity of convective cores come to ground several kilometers away from its source region (i.e., generated in one pixel but detected in a different pixel). Although it is not uncommon for ground flashes to propagate several kilometers in the horizontal direction before ultimately terminating at the ground, the horizontal resolution of the analysis grid may add to the observed scatter, and (2) due to the principles of radar operations. Here, aside from the assumptions inherent in the choice of Z-M relationship used in this study (addressed above), radar beam geometry coupled with the interpolation process can result in uneven smoothing of reflectivity data, as pixel sampling degrades with increased range from the radar.

One method of minimizing the effects of this "noise floor" scatter, in a statistically meaningful way, is to present the data in the form of binned scatter plots. Figures 3a and 3b examine mean IM values binned as a function of FD for each Eulerian analysis method, while in Figure 3c the mean cell total IMs are binned as a function of FCs per tracked cell in the CT method. Here, means and standard deviations (error bars) of IM samples falling in each FD/FC bin are plotted relative to the center of each bin interval. For sample sizes similar to those in this study, Wilkes [1995] suggests 20-25 class intervals, as an appropriate number of bins to represent the dataset; caution must be exercised to ensure that an adequate number of samples exist in each of the bins to allow for statistically meaningful calculations. To address this issue, we have elected to use the statistics of the FD and FC distributions to divide the FD and FC bins into 20 variable sized intervals, each specific to the chosen analysis method. In all cases, the first bin is associated with the mean IM for pixels / cells containing no lightning (i.e., FC = FD = 0). The cumulative distribution functions (CDFs) of the conditional FD grid points and FC cells (each conditioned on the occurrence of CG lightning) were then used to ensure that approximately the same number of data-pairs were present in each of the remaining class intervals. This approach ensured that statistics computed within each bin were done with similar sample sizes, thereby increasing the number of statistically meaningful bins. In the case of the EN and TI methods, non-lightning producing pixels (i.e., pixels in the first bin interval) equated to 55% and 0.1% of the CDF of FD grid points, respectively; the remaining 19 bins each contain roughly 3-8% of the remaining conditional FD grid points based on their respective CDFs (at least 679 and 587 points in each bin, respectively). In the CT method, however, over 90% of the tracked cells had no CG lighting associated with them, thereby requiring a slightly different approach in the division of the remaining 19 bins. Here, the second bin interval represents cells

that had exactly one ground flash associated with them, the third and fourth bins being associated with cells producing 2-4 and 5-9 flashes respectively, with the remaining 16 bins each containing approximately 4-9% of the remaining data-pairs associated with lightning producing cells (at least 601 points in each bin). The final bin interval presented in Figures 3a – 3c are each associated with the 95th percentile of the CDFs of their respective conditional FD / FC distributions. That is to say that the final class interval is truncated such that the data-pairs associated with the largest 5% of the FDs / FCs were excluded from the analyses.

Clearly, Figures 3a and 3b show strong linear relationships between column integrate ice and ground flash densities for our *Eulerian* analyses, with Figure 3c corroborating these findings from a cell-by-cell perspective. Overall, the slopes of best fit lines through the mean IM values in each bin, presented in Figures 3a – 3c, are fairly similar, all with non-zero intercepts suggestive of the presence of a minimum threshold IM value required for the occurrence of CG lightning. For these plots, data are correlated at levels in excess of R = 0.97 (0.978, 0.991 and 0.995 for EN, TI and CT methods, respectively).

4. Conclusions

Examining over 46,000 daytime volumes of convective WSR-88D radar data, this study investigated the relationship between radar derived precipitation ice mass and CG lightning over the period of 7 summer seasons (1997 – 2003). Whether examining observations of CG lightning and derived ice mass in a climatological (*Eulerian*) fashion, or doing so on a cell-by-cell basis, our findings corroborate those of previous investigators [e.g., Workman and Reynolds, 1949; Larsen and Stansbury, 1974; Carey and Rutledge, 2000; Petersen et al., 2005], firmly

establishing a link between a storms ability to generate enhanced concentrations of precipitation sized ice particles in the mixed-phase region, and its ability to generate lightning.

Based on solid physical arguments and the synthesis of this and numerous previous studies (referenced above), we have every reason to believe that this strong correlation is also causal. Therefore, relative to the documented anomaly in summer season ground flash densities over and around the Houston area [i.e., Gauthier et al., 2005], this implies that *the unique aspects of the Houston urban area must first generate an anomaly in convective intensity and precipitation ice, which then generates an anomaly in lightning. Hence, hypotheses offered to explain such an anomaly must be capable of (a) explaining either increased frequency and/or intensity of convection and (b) relating (a) to the enhancement of ice mass and lightning production.*

Finally, although total lightning data would prove to be a more complete estimate of the electrical strength of a thunderstorm, the strong linear relationship between column integrated precipitation ice mass and CG lightning, coupled with the robust statistics available from a dataset of this magnitude open the door for the assimilation of lightning data into mesoscale models. Here one could envision the relationships between precipitation ice and lightning being used to "nudge" the initialization of model ice fields such that the model more accurately represented the observed state of the atmosphere. In addition to a better initial model state, such an endeavor could ultimately lead the generation of forecast products identifying areas favorable for the development of lightning, thereby increasing critical warning lead times and enhancing public safety.

Acknowledgments. Post-processed lightning data were provided by the *NASA Lightning Imaging Sensor (LIS) instrument team and the LIS data center via the Global Hydrology Resource Center (GHRC) through a license agreement with Global Atmospherics, Inc (GAI).*

REFERENCES

Black, R. A. (1990), Radar reflectivity-ice water content relationships for use above the melting level in hurricanes, *J. Appl. Meteorol., 29*, 955–29,961.

Carey, L. D. and S. A. Rutledge (2000), The Relationship between Precipitation and lightning in tropical island convection: A C-band polarimetric radar study, *Mon. Wea. Rev., 128,* 2687–2710.

Cummins, K. L., M. J. Murphy, E. A. Bardo, W. L. Hiscox, R. B. Pyle, and A. E. Pifer (1998), A combined TOA/MDF technology upgrade of the U.S. National Lightning Detection Network, *J. Geophys. Res., 103*(D8), doi: 10.1029/98JD00153.

Dixon, M. and G. Wiener (1993), TITAN: thunderstorm identification, tracking, analysis, and nowcasting—A radar-based methodology, *J. of Atmos and Ocn Tech., 10*, 785–797.

Kalnay, E., et al. (1996), The NCEP/NCAR 40-year reanalysis project, *Bull. Amer. Meteor. Soc., 77,* 437–471.

Larson, H. R. and E. J. Stansbury (1974), Association of lightning flashes with precipitation cores extending to height 7 km, *J. Atmos. Terr. Phys., 36*, 1547-1553.

MacGorman, D. R., and W. D. Rust (1998), *The Electrical Nature of Storms,* 422 pp., Oxford Univ. Press, New York.

Orville, R. E., G. Huffines, J. Nielsen-Gammon, R. Zhang, B. Ely, S. Steiger, S. Phillips, S. Allen, and W. Read (2001), Enhancement of cloud-to-ground lightning over Houston, Texas, *Geophys. Res. Lett., 28*(13), doi:10.1029/2001GL012990.

Petersen, W. A. (1997), Multi-scale process studies in the tropics: Results from lightning observations, *Ph.D. dissertation, Department of Atmospheric Science, Colorado State University, 632,* 354 pp.

Petersen, W. A., and S. A. Rutledge (2001), Regional variability in tropical convection: Observations from TRMM, *J. Clim., 14,* 3566–3586.

Petersen, W. A., H. J. Christian, and S. A. Rutledge (2005), TRMM observations of the global relationship between ice water content and lightning, *Geophys. Res. Lett., 32,* L14819, doi:10.1029/2005GL023236.

Reap, R. M. (1986), Evaluation of cloud-to-ground lightning data from the western United States for the 1983–84 summer seasons. *J. of Appl. Meteor., 25*, 785–799.

Saunders, C. P. R., W. D. Keith, and R. P. Mitzeva (1991), The effect of liquid water on thunderstorm charging, *J. Geophys. Res., 96,* 11,007–11,017.

Steiger S. M., R. E. Orville, and G. Huffines (2002), Cloud-to-ground lightning characteristics over Houston, Texas: 1989–2000, *J. Geophys. Res., 107*(D11), doi:10.1029/2001JD001142.

Takahashi, T. (1978), Riming electrification as a charge generation mechanism in thunderstorms, *J. Atmos. Sci., 35*, 1536-1548.

Wilkes, D. S. (1995), *Statistical Methods in the Atmospheric Sciences*, 465 pp., Academic Press, San Diego, CA.

Workman, E. J. and S. E. Reynolds (1949), Electrical activity as related to thunderstorm cell growth, *Bull. Amer. Meteor. Soc.*, *30*, 142-149.

CAPTIONS

Figure 1. Seven-year (1997-2003) summer season ground flash density anomalies created by normalization of mean flash densities of each pixel by the domain mean (shaded contours); values > 1 indicate positive anomalies and values < 1 negative anomalies. Corresponding anomalies in radar derived ice mass are overlaid as white contours.

Figure 2. Scatter plots of the warm-season convective IM as a function of FD for (a) volume total IM – the "ensemble" method [EN] and (b) time-integrated [TI] mean IM for each 2 km pixel. Panel (c) presents similar results for the cell tracker [CT] analysis, with cell total IM (abscissa) presented as a function of cell flash count (FC, ordinate). The number of samples (n) contained in each figure, as well as the linear correlation coefficient (R) are included with their respective panels.

Figure 3. Average convective IM (ordinate) occurring in each lighting FD bin (abscissa) for: (a) EN radar volume samples and (b) TI pixel samples, with (c) average cell total IM occurring in each cell FC bin. In all cases, the first bin interval is associated with non-lightning events (i.e., FD = FC = 0), with remaining variable sized bin intervals each encompassing roughly 5-10% of the remaining data pairs; data points are plotted relative to the interval mid-point, horizontal bars represent bin widths, vertical error bars associated with ± 1 standard deviation for each data point.

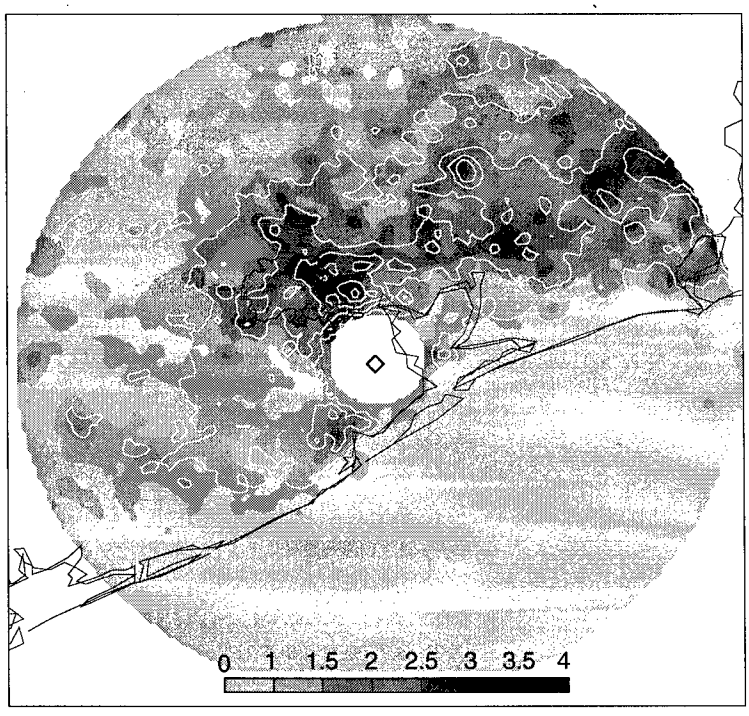

Figure 1. Seven-year (1997-2003) summer season ground flash density anomalies created by normalization of mean flash densities of each pixel by the domain mean (shaded contours); values > 1 indicate positive anomalies and values < 1 negative anomalies. Corresponding anomalies in radar derived ice mass are overlaid as white contours.

Error!

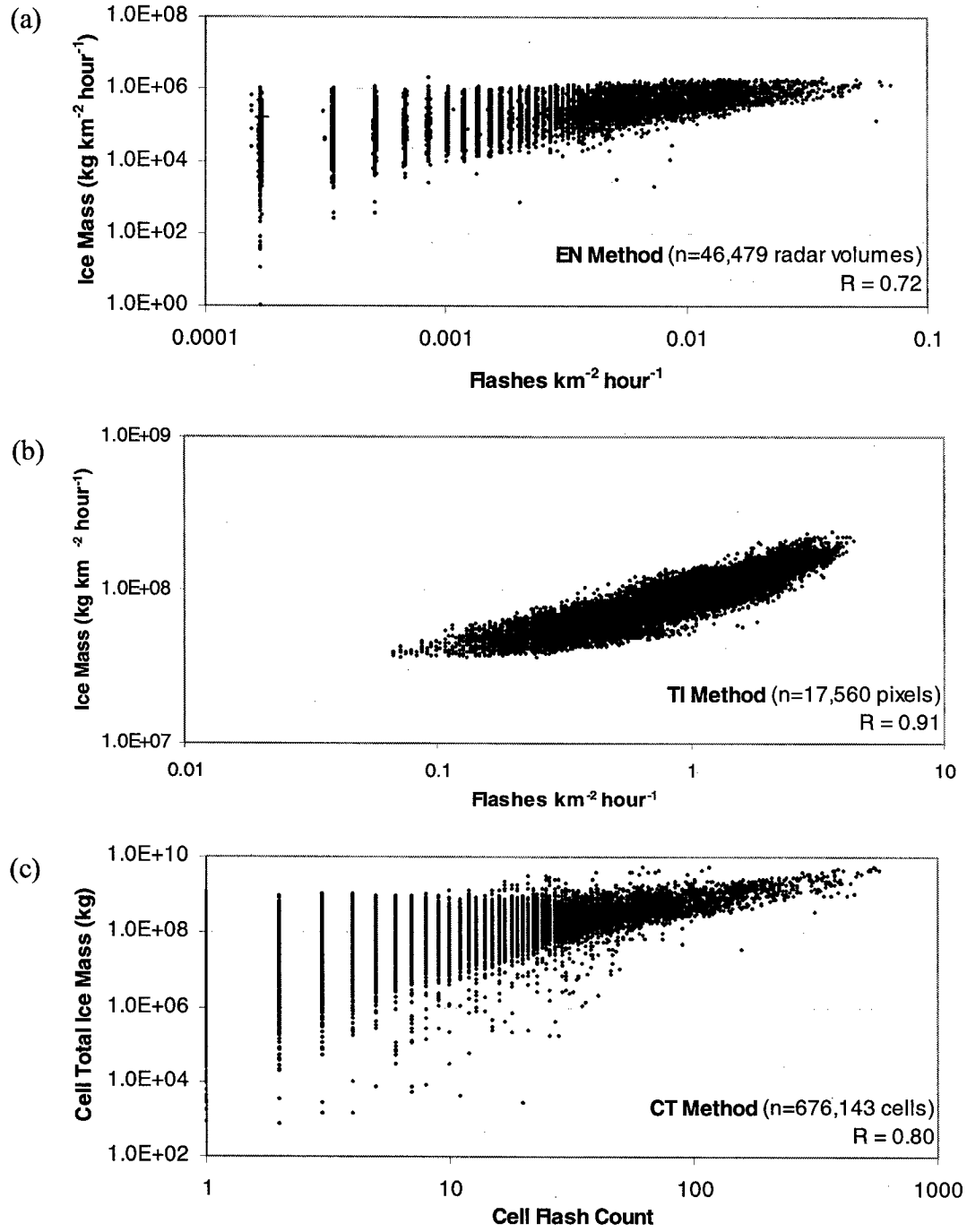

Figure 2. Scatter plots of the warm-season convective IM as a function of FD for (a) volume total IM – the "ensemble" method [EN] and (b) time-integrated [TI] mean IM for each 2 km pixel. Panel (c) presents similar results for the cell tracker [CT] analysis, with cell total IM (abscissa) presented as a function of cell flash count (FC, ordinate). The number of samples (n) contained in each figure, as well as the linear correlation coefficient (R) are included with their respective panels.

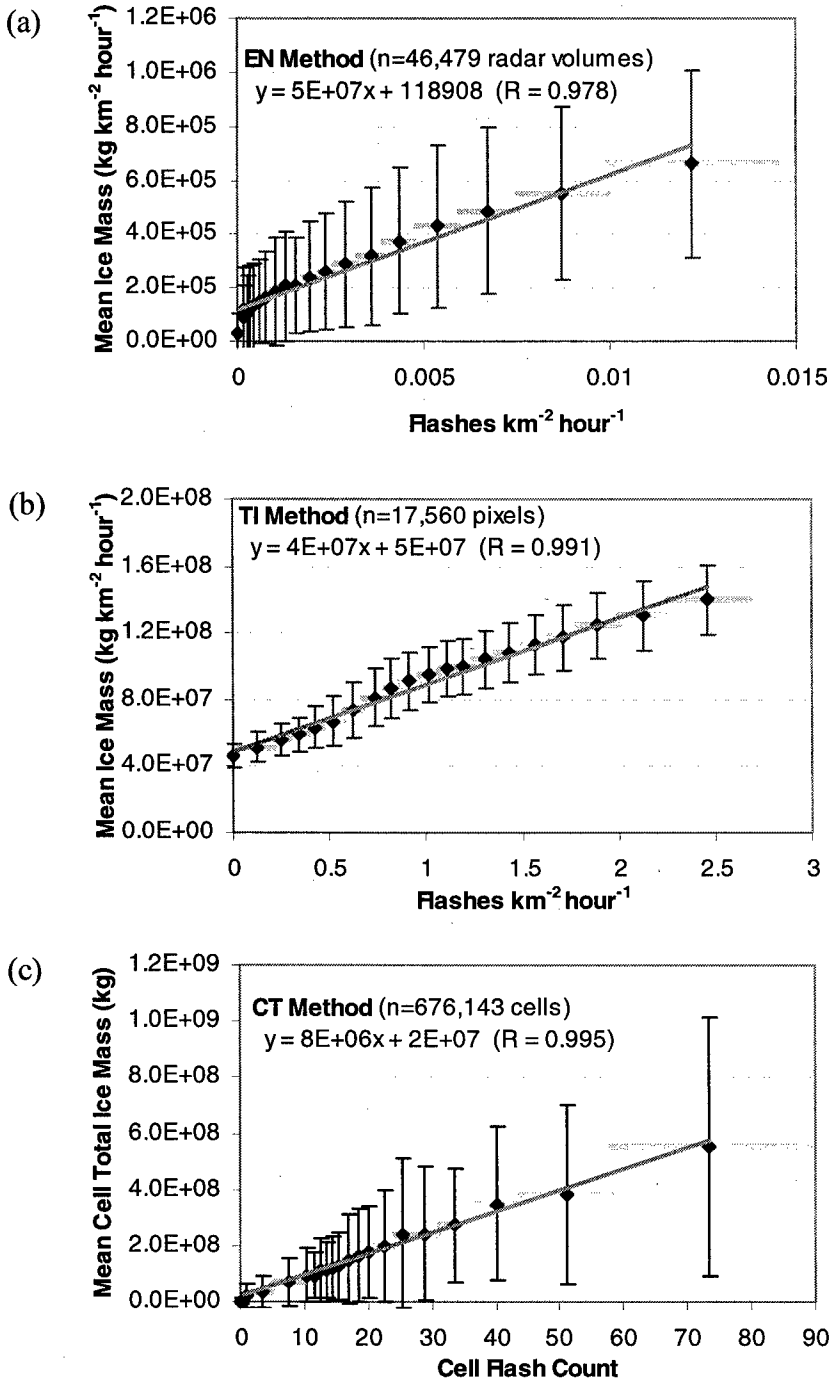

Figure 3. Average convective IM (ordinate) occurring in each lighting FD bin (abscissa) for: (a) EN radar volume samples and (b) TI pixel samples, with (c) average cell total IM occurring in each cell FC bin. In all cases, the first bin interval is associated with non-lightning events (i.e., FD = FC = 0), with remaining variable sized bin intervals each encompassing roughly 5-10% of the remaining data pairs; data points are plotted relative to the interval mid-point, horizontal bars represent bin widths, vertical error bars associated with ± 1 standard deviation for each data point.